https://doi.org/10.15407/ujpe70.4.251

N.V. BONDAR, 1 YU.P. PIRYATINSKI, 2 O.V. TVERDOCHLIBOVA 1

- ¹ Institute of Physics, Nat. Acad. of Sci. of Ukraine, Department of Nonlinear Optics (46, Nauky Ave., Kyiv 03028, Ukraine)
- ² Institute of Physics, Nat. Acad. of Sci. of Ukraine, Department of Molecular Photoelectronics (46, Nauky Ave., Kyiv 03028, Ukraine)

COMPARISON OF OPTICAL AND ENERGY CHARACTERISTICS OF EXCITONS IN AQUEOUS SOLUTIONS AND SOLID FILMS OF QUANTUM DOTS

The results of studies of colloidal solutions of ultra-small ZnSe quantum dots (QDs) stabilized by short thioglycerol molecules and their dense films, which constitute the material basis of optoelectronic structures, are reported. A comparison of the results obtained for the solutions and the films makes it possible to better understand the transformation of corresponding optical characteristics during the transition from a system of non-interacting particles in the solution to a system with strong interaction between QDs. Delocalization of excitons and hybridization of their wave functions create a new set of QD energy states in the films, which govern the transport and optical properties of the latter. A substantial red shift between the absorption spectra of the solution and the film has been revealed, the nature of which is determined by strong interaction among the QDs. The researched dynamic characteristics showed that the time of the exciton excitation energy transfer in the films of ZnSe DQs with strong interaction can be subnanosecond (≈ 610 ps) and dominate over the time of internal exciton relaxation into in-gap, surface, and defect states of charge carriers.

Keywords: Stokes shift, quantum dot, excitation energy, exciton, ZnSe.

1. Introduction

Quantum dots (QDs) are semiconductor nanocrystals confined in all three dimensions. As a result, we can systematically vary their optical properties by changing their size [1]. Due to their unique properties, QDs are promising materials for producing light-emitting diodes (LEDs) [2], lasers, photovoltaic structures [3], and in photocatalysis [4], as well as a platform for

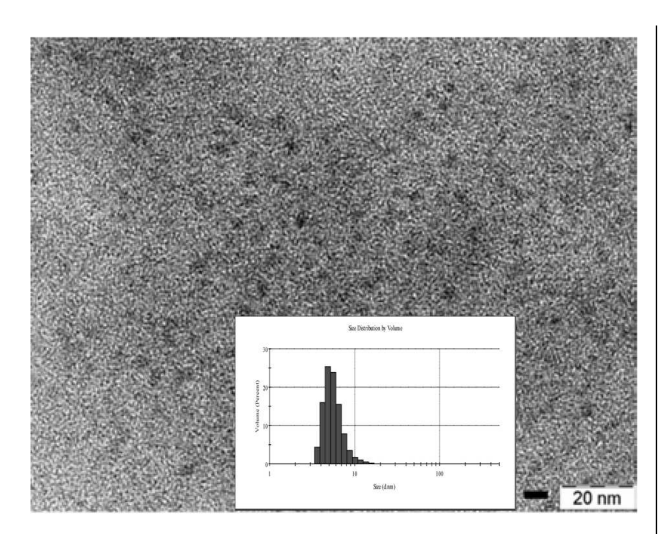
Citation: Bondar N.V., Piryatinski Yu.P., Tverdochlibova O.V. Comparison of optical and energy characteristics of excitons in aqueous solutions and solid films of quantum dots. *Ukr. J. Phys.* **70**, No. 4, 251 (2025). https://doi.org/10.15407/ujpe70.4.251.

ISSN 2071-0186. Ukr. J. Phys. 2025. Vol. 70, No. 4

studying the phenomenon of excitation energy transfer [5]. The material basis of the mentioned systems consists of solid, densely packed QD films, the surfaces of which are covered with ligand molecules to prevent their aggregation.

Since dense QD films and superlattices are formed from the liquid phase, the optical and transport properties of charge carriers in them are determined by the characteristic properties of electrons and holes in QD colloidal solutions. In practice, as a rule, either a dilute QD solution or a solid film is studied, so the corresponding results are rarely compared with each other. For example, the origin of such a phenomenon as the Stokes shift (the difference between the maxima of the absorption and emission spectra) has been studied mainly in dilute QD solutions [6–11]. Howe-

[©] Publisher PH "Akademperiodyka" of the NAS of Ukraine, 2025. This is an open access article under the CC BY-NC-ND license (https://creativecommons.org/licenses/by-nc-nd/4.0/)



 $Fig.\ 1.$ TEM image and histogram (the inset) of the size distribution of ZnSe QDs according to DLS data; scale bar equal 20 nm

ver, to our knowledge, there are no studies that show the transformation of optical characteristics from the solution to the QD-film ones, which occurs due to the transition from a non-interacting system to a system with strong exciton interaction between the QDs.

Another problem is the relaxation of hot or cold excitons in single QDs and QD films, and how strong interaction associated with high kinetic energy of excitons and short ligand molecules [12–15] affects this parameter.

In this paper, we report the results of our studies concerning stationary and time-resolved optical spectra of ZnSe QD dilute solutions and solid films, and analyze the nature of the transformation of their characteristics when changing from one system to the other. One of the important obtained results is the identification and justification of the origin of the red shift taking place between the absorption spectra of QDs in the solution and the film and caused by the hybridization of exciton quantum states, and the explanation of the origin of the Stokes shift in QD solutions and films.

Another result concerns the dynamic relaxation processes of hot excitons in single QDs and QD films. We have found that provided the same excess excitation of the solutions and the films, the rates of exciton relaxation to the ground and surface states due to the energy transfer between QDs are an order of magnitude higher than those of the internal relax-

ation to analogous states in single QDs. The obtained results provide an understanding of the exciton relaxation pathways in ultrasmall ZnSe QDs and their possible approximation in photovoltaic structures and light-harvesting antennas [3, 4].

2. Experimental Part

The synthesis of colloidal water-soluble QDs for the fabrication of solid-film devices may be more environmentally friendly than the preparation of QDs in organic solvents for the same purpose due to the larger simplicity and the lower cost of the procedure [1]. ZnSe QDs covered with short thioglycerol (TG) molecules, which are studied in this work, were synthesized in aqueous solutions according to the protocol outlined in some of our previous articles [9, 13, 14]. The molar ratio of Zn, Se, and TG determined as 1.1:0.57:2.7, but was experimentally changed to the optimal value 2:1:2.5.

We prepared two samples of QD solutions with the average QD radii $R_{1(2)}=1.5(1.2)\pm0.1$ nm. The latter were determined by measuring the hydrodynamic diameter (dynamic light scattering, Zetasizer Nano ZS) [14]. Thus, taking into account that the length of the TG ligand molecule equals $\lambda\approx0.75$ nm [13], the QD center-to-center distance was 3.75 nm (3.15 nm). In such ultrasmall QDs, excited electrons and holes are in a strongly quantized regime with a high initial kinetic energy because the Bohr radius of exciton in ZnSe is $a_x\approx3.7$ nm.

Between 5 and 10% remain unavoidable. If we consider the shape of synthesized QDs in our specimens to be spherical, then the standard deviation (the standard variance) of their diameter was about 8%. This value was determined by counting approximately a hundred QDs in a typical image obtained using a transmission electron microscope (TEM).

It should be noted that for ultrasmall ZnSe QDs, the low contrast between them and the substrate strongly complicated their counting and the determination of dispersion, as can be seen in Fig. 1. The figure also demonstrates a histogram of the QD size distribution, which can be well approximated by the Gaussian function.

QD films were formed by heating them in air at the temperature $T\approx 50$ °C until the aqueous solution completely evaporated; see Fig. 2, a. However, the quality of their surface became substantially worse at $T\geq 80$ °C through the formation of agglomer-

ates, cracks, and cavities, as one can see by comparing Figs. 2, a and 2, b obtained using an optical microscope (Leica microscopes (the inVia system)).

To confirm the obtained QD sizes, absorption spectra (the value of the first exciton transition), the effective-mass model in a spherical potential, and the particle-in-a-sphere model were additionally used.

To obtain densely packed films, a concentrated QD solution were deposited on quartz substrates by a layer-by-layer spin-coating procedure. As a result, a film with a thickness of about 50 nm was obtained. Then the process was repeated several times until the film thickness reached a value of about 500 nm. The average thickness of the produced QD films was estimated using a Tencor Alpha-Step D-500 Profilometer (Tencor-Instruments).

Experiments dealing with ultraviolet (UV)-visible (Vis) absorption and stationary and time-resolved photoluminescence in QD solutions (a square transparent quartz cuvette with an optical path length of 10 mm) and films were carried out at room temperature using SHIMADZU UV-2450 and Life Spec-II spectrophotometers (Edinburgh Instruments Ltd). To excite the PL signal in the UV-vis region, a pulsed LED with the wavelength $\lambda = 255 \text{ nm} \ (\approx 40 \ \mu\text{W})$ and the instrument response function (IRF) of about 900 ps, as well as a picosecond pulsed diode laser EPL-405 with $\lambda = 405$ nm (≈ 5 mW, IRF ≈ 280 ps), were used. Excitation photoluminescence PLE and TRPL spectra were also registered using the following spectrophotometers as excitation sources: an FS-5 spectrophotometer (Edinburgh Instruments Ltd) with a Xenon lamp (≈ 150 W), a pulsed LED with $\lambda = 375 \text{ nm} (IRF \approx 800 \text{ ps}), \text{ and a Perkin-Elmer}$ Lambda LS-55 spectrophotometer (Perkin–Elmer Instruments, UK). The pump intensity was kept low to avoid multiexciton absorption and inevitable Auger heating of single QDs.

3. Results and Their Discussion

3.1. Stokes shift and medium effect on optical and energy spectra of ultrasmall ZnSe quantum dots

Unfortunately, the quality of QDs of II–VI semiconductors grown in aqueous solutions at low temperatures is lower (they have more defects) in comparison with those obtained via the non-aqueous high-temperature synthesis in organic solvents [1]. Despite



a

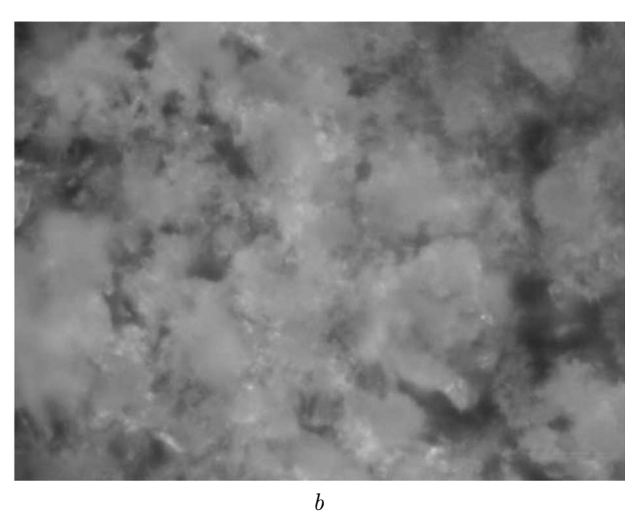
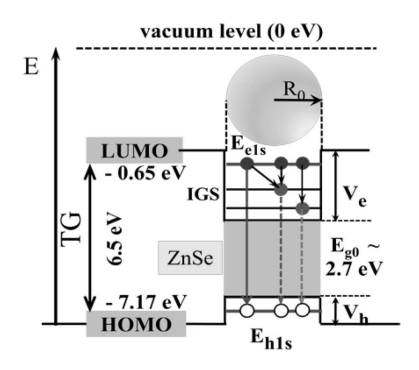


Fig. 2. Images of the surface of ZnSe QD films heated to 50 °C (a) and 80 °C (b) for 2 h; scale bar equal 5 μm

this fact, the synthesis of colloidal QDs in water remains attractive due to the possibility of using environmentally friendly materials.

Being covered with molecules of appropriate ligands, which regulate their growth and prevent their agglomeration, QDs form complexes of the first (type-I) or second (type-II) type, whose energy pictures are one of the main characteristics [16]. In the former (type-I) case, the width of the HOMO (the highest occupied molecular orbital)—LUMO (the lowest unoccupied molecular orbital) gap of the ligand completely overlaps the counterpart value for QDs, where the excited electrons and holes are localized. In the latter (type-II) case, the corresponding forbidden gaps in



Scheme 1. Positions of the HOMO–LUMO levels in TG (with respect to the vacuum level) calculated using the density functional method, and the energy structure of ZnSe QDs with the corresponding values of the potential wells for electrons and holes

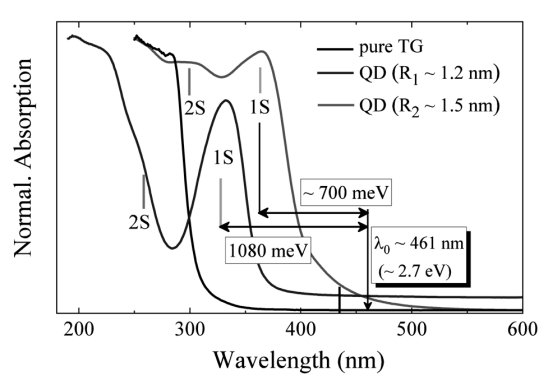


Fig. 3. Raw absorption spectra of pure TG and ZnSe QDs with radii $R_{1,2}$. The vertical colored lines mark the maximums of the Gaussian functions that approximate the corresponding ASs. The double-head arrows marked as ~ 1080 meV and ~ 700 meV denote the energy shifts of 1S excitons due to the quantum-size effect in QDs with R_1 and R_2 , respectively. The vertical black line at about 434 nm marks the maximum of the I_{2s} band

the QD and the ligand are energy-shifted with respect to each other, which leads to the spatial separation of electrons and holes and their localization in the QD and the ligand.

As a rule, Zn-chalcogenides are doped with thiols. The latter, as ligands of the X-type, bind to the chalcogenide surface due to the affinity of the thiol group with respect to Zn-chalcogenides, thus providing a chemical bond with Zn²⁺ at the QD surface; as in our case ZnSe QD + TG [17]. Unlike the latter, the energy picture in similar complexes CdSe QD + thiols belongs to the second-type structures, where ligands

are hole acceptors that capture excited holes from the QDs; as a result, we obtain a spectral (bathochromic) shift of the PL band and its rapid decay [18].

The positions of the conduction and valence bands with respect to the vacuum level are well known to date for most II-VI semiconductors, including ZnSe. At the same time, the determination of the corresponding HOMO-LUMO levels in organic ligands is a difficult task. In our previous works [13, 14], the density functional method (B3LYP DFT-D4 package, 6-31++G(3d,3p,f)) was used to calculate the corresponding TG levels. To determine the average QD radius, we applied the particle-in-a-sphere model, which is a basis for calculating the energies of absorption peaks and the line width (see Scheme 1). The obtained value of the ratio between the potential well energies for electrons and holes equals $V_e/V_h \approx 12.6$, which made it possible to calculate the positions of the $(1S_e - 1S_h)$ and $(1S_e - 2S_h)$ exciton levels in the corresponding QDs.

Figure 3 demonstrates the raw absorption spectra (AS) of two colloidal QD solutions with $R_{1(2)} =$ = 1.5(1.2) nm and pure TG, where the molar concentrations of QD and TG were identical. To determine the positions of the 1S and 2S absorption peaks more accurately, the shapes of the AS curves were fitted by Gaussian functions (their maxima are marked with vertical colored lines), which agreed well with the calculated and experimental data, as well as with similar results of other authors [19–23]. It can be seen from the figure that due to the strong quantum-size effect, the blue shift of the absorption bands in ultrasmall ZnSe QDs equals about 0.7 and 1.080 eV for larger and smaller, QDs, respectively, with respect to the ZnSe band gap width $\lambda_0 = 461 \text{ nm}$ $(\approx 2.7 \text{ eV})$. This circumstance provides a high initial kinetic energy of excitons in QDs, which is important for the exciton energy transfer in light-harvesting antenna complexes and photovoltaic structures (solar cells) [24].

The AS of pure organic ligands and QDs bound to surface atoms are different, so the experimental AS peaks may not correspond to the calculated ones, which is typical of the UV region, where the bands overlap quite strongly, as is shown in Fig. 3. To obtain accurate peak energy values and the AS shapes for separate QDs, we subtracted the AS of pure TG from the corresponding spectra of QD solutions, which are shown in Fig. 4 together with the PL spectra. The

demonstration of the AS and PL spectra in the same figure has advantages over their separate presentations because it allows a comparison of the characteristic positions of one spectrum with those in the other spectrum to be made. The absorption curves obtained for both samples (dashed curves (magenta) in Fig. 4) now represent the AS of pure QDs, whose shapes were also fitted by Gaussian functions. The maximums of the latter coincide well with their counterparts in Fig. 3.

Figure 4, in addition to the general shape of the AS, also exhibits the 1S absorption lines (black dashed curves), and the maxima of the others are marked by vertical (orange) lines: 1S (363 nm (3.41 eV)) and 2S (299 nm (4.14 eV) for QDs with R_1 , and 1S(327 nm (3.79 eV)) and 2S (259 nm (4.78 eV)) for R_2 . The vertical arrow at about 260 nm in Fig. 4, amarks the beginning of the continuum. The vertical lines at about 434 nm (2.85 eV) in Figs. 3 and 4, amark the maximum of the I_{2s} band of in-gap states (IGSs). The latter were mentioned in our previous works [13, 14]. They form the low-energy shoulder of the AS of QDs with R_1 and lead to its broadening. As a result, the full-width-at-half-maximum (FWHM) ratio between the 1S AS curves for both specimens equals 57 nm/46.8 nm ≈ 1.2 .

Figure 4 also shows the PL spectra of the solutions of both QD samples excited by an LED with $\lambda=255$ nm. It should be noted that a characteristic feature of ultrasmall QDs is the increase of the ratio between the numbers of the surface atoms and the internal ones, which manifests itself in the broad shapes of the overall PL spectra of both samples. When they are excited with an excess energy higher than 1 eV, hot excitons are created, which quickly relax and populate mainly the surface and defect states in QDs. The PL intensity from those states substantially exceeds that from quantum states, as can be seen in Fig. 4.

The shapes of the PL spectra can be optimally fitted using five Gaussians, which we divided into three groups: the Q band, which arises owing to band-to-band recombination of electrons and holes in the quantum states; the I_{1s} and I_{2s} bands ("s" means surface), which are related to the IGS states; and the D and H bands, which are formed by surface defects (vacancies, stacking faults, etc.). The latter are responsible for the green and orange emission in the visible spectrum [22, 23]. Therefore, in

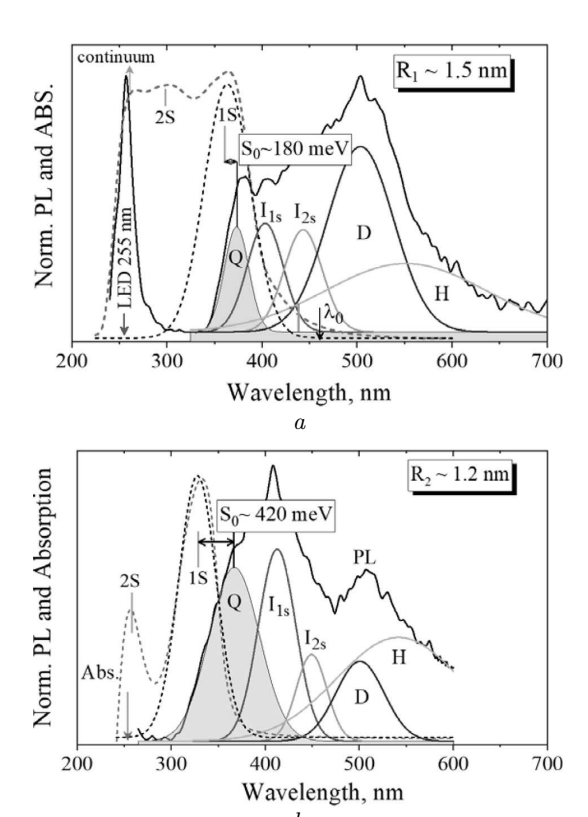


Fig. 4. Absorption (AS) and photoluminescence (PL) spectra of colloidal QD solutions with $R_1 \approx 1.5$ nm (a) and $R_2 \approx 1.2$ nm (b) excited by an LED with $\lambda = 255$ nm (4.86 eV) and the resolutions of the PL spectra into Gaussian curves $(Q, I_{1s}, I_{2s}, D, \text{ and } H)$. The corresponding Stokes shifts S_0 are indicated. The AS were obtained by subtracting the raw pure TG spectrum from the corresponding QD spectra (see the text)

what follows, we will focus attention only on the first three bands.

The nature of the I_{1s} and I_{2s} bands is the most difficult to explain, and the reason for their formation in QDs is still debated. The authors of work [25] have proposed an interesting model where the formation of IGS levels of electrons and holes was explained as a result of a considerable difference (more than an order of magnitude) between the effective masses of charge carriers in the QD materials and the ligand molecules. In this case, the dependence of the IGS energy levels on the QD size would be different than that for internal excitons. However, as far as we know, this model has not been experimentally confirmed.

As was noted in works [6, 26–28], the main role in the appearance of IGS states is played by the aqueous environment, the molecules of which hydroxylate the

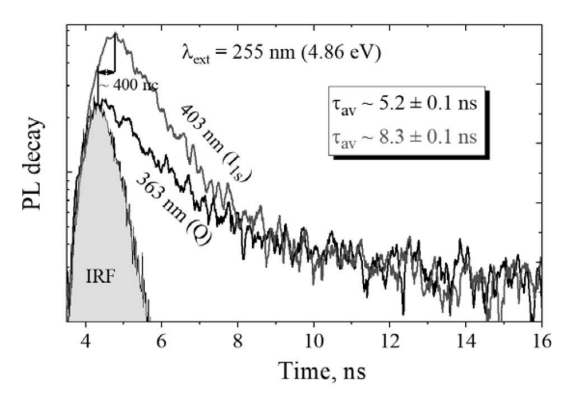


Fig. 5. Profiles of PL decay in a colloidal QD solution registered at wavelengths of 363 nm (Q band) and 403 nm (I_{1s} band). Excitation with $\lambda_{\rm exc}=255$ nm. The average decay times ($\tau_{\rm av}$) were obtained by approximating the profiles with a double-exponential function

surface of ZnSe QDs through dissociative chemisorption during their synthesis, and owing to the H⁺, OH⁻, and H₂O inclusions can introduce surface trap states. Zaiping Zeng *et al.* [26, 27], by combining theoretical and experimental results, showed that two types of IGS levels can exist in ZnSe QDs depending on the configuration between Zn, O, Se or Zn–OH atoms.

We have noted these results in our previous works [9, 14], and to confirm them, we prepared ZnSe QD samples of two sizes, which also demonstrate these bands in the QD band gap. In both samples, they lie in a narrow spectral interval with an average distance between them of 250 ± 10 meV. These bands are synchronously shifted to the red side by (7 ± 1) nm in QDs with R_2 , as can be seen from Fig. 4, b. However, at present, we cannot state that this is a consequence of quantum-size dependence. In addition, the presence of the I_{2s} state is confirmed by the broadening of the AS of the solution with R_1 (Fig. 3). At the same time, in the solution with R_2 , this broadening is small due to a substantial blue shift of the AS. The I_{1s} and I_{2s} bands have almost the same FWHM values with the ratios FWHM1.5 (I_{1s}) /FWHM1.2 $(I_{1s}) \approx$ $\approx 1 \pm 0.1$ and FWHM1.5 (I_{2s}) /FWHM1.2 $(I_{2s}) \approx 1.1 \pm$ ± 0.1 , whence we may assume that the total number of IGS states is determined by the QD growing conditions and, probably, remains constant if the QD size changes.

A characteristic feature of both PL spectra in Fig. 4 is a large Stokes shift, whose origin is still debated despite that this phenomenon has been studied

for a long time in various QDs (CdSe, PbS, PbSe, CsPbBr₃, and others) [7–11]. Various authors proposed several reasons for the formation of the Stokes shift: the Franck–Condon shift, exchange interaction, polydispersity of QD sizes and IGS states [7, 8]. Another model, which explains this phenomenon and is based on a tight-binding approach, describes the shift as a consequence of splitting between bright and dark exciton states [10, 11]. However, these models can explain only (10–30) meV of the shift magnitude, but not >100 meV, which is observed in our experiment.

The difficulty in determining the nature of this phenomenon in QDs consists in that both the AS and PL band depend, although in different ways, on the QD size. It can be seen from both panels that the shift value increases from 180 to 420 meV mainly due to the AS shift in both specimens, i.e., owing to the quantum-size effect of excitons, as was emphasized in work [8]. For ultrasmall QDs, the blue shift of the Q band is insignificant as compared with its broadening, which can be estimated by the ratio FWHM1/FWHM2 = 0.5 for QD size ratio $R_1/R_2 \approx 1.25$.

The origin of the Q band broadening is the increase of the number of surface atoms in comparison with the internal ones when the QD size decreases. Another possible origin of the Stokes shift is a large dielectric mismatch between the ZnSe materials ($\varepsilon \approx 9$) and the aqueous solution ($\varepsilon \approx 80$), which induces a bathochromic red shift of the PL band. Both factors reduce the confinement energy of excitons by weakening their quantum-size effect, increasing the wave function size, and thus giving rise to a strong broadening of the PL band.

At the end of this Subsection, we report the results obtained for the PL signal decay in single QDs in the solution due to internal dynamic processes. This phenomenon makes it possible to estimate the decay rate of the exciton population participating in those processes. In Fig. 5, two PL decay profiles are shown, which were measured in the QD solution with R_1 (similar profiles were registered for the solution with R_2) at the wavelengths $\lambda=363$ and 403 nm corresponding to the maximums of the Q and I_{1s} bands. To prevent interaction between QDs, the colloids were substantially diluted.

The profiles are well approximated by a double-exponential function:

$$I(t) = A_1 \exp(-t/\tau_1) + A_2 \exp(-t/\tau_2) + A_0,$$

ISSN 2071-0186. Ukr. J. Phys. 2025. Vol. 70, No. 4

where $A_{0,1,2}$ are amplitudes, and $\tau_{1,2}$ are decay times. The calculated average decay times

$$\tau_{\rm av} = \frac{A_1(\tau_1)^2 + A_2(\tau_2)^2}{\tau_1 + \tau_2}$$

are indicated in Fig. 5. Two exponential functions describe the decay of the exciton population within the time window of our measurements (50 ns). The quantity

$$\gamma = \frac{A_1+A_2}{A_1+A_2+A_0} \approx 99\%$$

testifies that, within these limits, almost all excitons in the corresponding states decay.

Excitation with a large excess of energy (4.86 - 3.41 = 1.45 eV) leads to the excitation of excitons in both states, Q and I_{1s} . The former decays by transferring some of its energy to the latter, whose population reaches a maximum after about 400 ps. This is a consequence of a considerable overlap of the wave functions of both exciton states and different decay rates, which can be seen from Fig. 5. Below we will show that the reported optical and energy characteristics of single QDs in solutions undergo changes in films as a result of excitonic interaction between QDs, which affects the transfer of excitation energy in systems with energy and spatial disorders.

3.2. Steady-state and time-resolved optical spectra of dense ZnSe QD films as a result of strong coupling between QDs

One of the important differences between the optical spectra of dilute QD solutions and densely packed solid QD films is the position of their absorption spectra. The coupling between the QDs in the film leads to the appearance of new electronic levels of excitons and, as a result, a red shift of the film AS with respect to that of the solution, which can be detected by comparing the ASs of the solution and the film. However, this is a difficult task because the excitonic interaction between QDs leads to a strong broadening of the film AS, which becomes featureless, so it is difficult to accurately determine excitonic peaks, as shown in Fig. 6.

In this case, the PL excitation (PLE) spectrum is more reliable when determining the energy levels of excitons. It resembles the PL spectrum, but

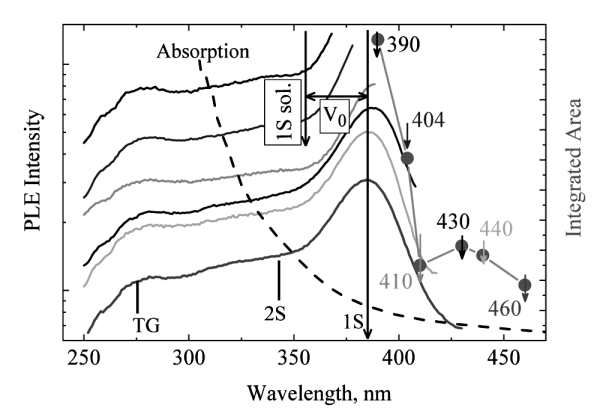


Fig. 6. Absorption and PL excitation (PLE) spectra for QD films with R_1 obtained at various detection λ_{det} (indicated in the figure). The large (dark yellow) circles indicate the integral areas of the corresponding PL bands (the right-hand side of the figure) and are marked by the value of V_0 , the difference between the 1S absorption states in the colloid and the film (short and long vertical arrows). The orange curve connecting the points is an eye guide

the detection wavelength $\lambda_{\rm det}$ remains fixed at a certain value, whereas the excitation wavelength $\lambda_{\rm exc}$ varies. The depicted in Fig. 6 PLE spectra were registered at various $\lambda_{\rm det}$'s, whose positions are indicated by short vertical arrows. The feature of the PLE spectrum is the $\lambda_{\rm det}$ -independence of its main band position 385 nm (3.22 eV), which is marked by a long black vertical arrow. It points to the fact that the quantum, IGS, and surface states of charge carriers are mainly populated from the same source rather than different ones. The obtained results differ from analogous ones obtained in work [29] for CdSe QDs covered with oleic acid, where the PLE peaks detected at the gap edge and in the surface state region were shifted with respect to each other.

To explain the transformation of excitonic states when changing from the QD solution to the QD film, the PLE band registered at $\lambda_{\rm det}=460$ nm (magenta) was approximated by Gaussian functions, whose maximums are marked by vertical black lines in Fig. 6. This approximation made it possible to determine the positions of the 1S and 2S states, as well as the energy level associated with the absorption of TG molecules at the QD surface. Fig. 6 shows, that the coupling between QDs leads to a red shift of the 1S and 2S excitonic levels by about 180 and 500 meV, respectively, in comparison with the analogous shifts in the QD solution. The evaporation of the aqueous

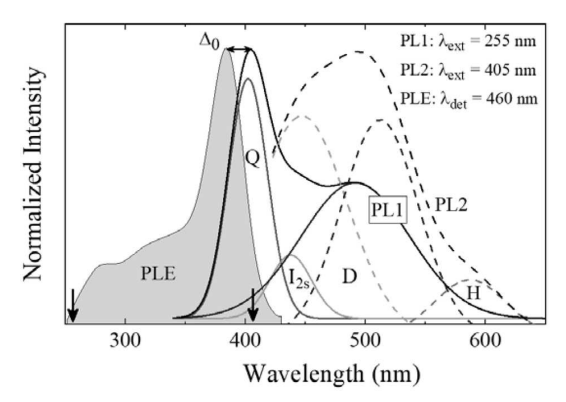


Fig. 7. PLE spectra ($\lambda_{\rm det} = 460$ nm, tinted band) and PL (PL1 and PL2) spectra of QD films excited at $\lambda_{\rm exc} = 255$ (the solid black curve) and 405 nm (the dashed black curve), marked by two thick arrows. The corresponding Gaussian profiles are shown (the solid and dashed colored bands Q, I_{2s} , D, and H), which approximate the corresponding PL spectra. The value $\Delta_0 \approx 160$ meV is the Stokes shift

solution during the QD film formation led to a band gap reduction for TG molecules on the QD surface and a red shift by about 250 meV.

On the right-hand side of Fig. 6, we showed (dark yellow dots) the $\lambda_{\rm det}$ -dependence of the normalized integral areas of the main PLE peak, which gives the ratio between the exciton populations in the quantum and IGS states. For example, the ratio between the areas at $\lambda_{\rm det} = 390$ and 430 nm equals 1:0.31 and gives the ratio between the PL intensities of the quantum and I_{2s} states.

The vertical arrows in Fig. 6 demonstrate the red shift $V_0 \approx 180$ meV of the PLE band with respect to the 1S level in the QD solution. As was explained above, this phenomenon is not associated with the difference between the absorption and emission of excitons, but related to the formation of new exciton states owing to the hybridization of wave functions with strong interaction between QDs [30, 31]. Resultantly, absorption in the film is performed not by ZnSe QD monomers, as it occurs in the solution, but by QD molecules (dimers, trimers, etc.). To estimate V_0 , we used the following expression that determines the strength of the dipole-dipole coupling between QDs [30, 32]:

$$V_0 = \frac{k \left| \mu_{DA} \right|^2}{n^2 d_{DA}^3},\tag{1}$$

where $|\mu_{DA}|^2 = 9.2 \times 10^{-3} \text{ M} \cdot \text{s} \cdot \text{D}^2 \times (n\varepsilon\Delta\nu/\nu)$ is the dipole moment (in debyes), $d_{DA} \approx a$ is the dis-

tance between the QDs, n is the refractive index of the medium (for TG, $n \approx 1.8$), and k is the orientation factor. For QDs with $R_1 = 1.5$ nm, the lowest 1S exciton level is 3.42 eV, FWHM ≈ 352 meV, the extinction coefficient $\varepsilon(3.42$ eV) $\approx 2 \times 10^5$ M⁻¹·cm⁻¹, and $\Delta \nu / \nu \approx 0.103$. As a result, we obtain $V_0 \approx 170$ meV, which agrees well with the experimental value.

The origin and magnitude of the Stokes shift in solutions were explained above however, in QD films, they is different. Figure 7 illustrates the PLE spectrum detected at $\lambda_{\text{det}} = 460 \text{ nm}$ (see also Fig. 6) and the PL spectra at excitation with $\lambda_{\rm exc} = 255$ nm (PL1, solid curves) and 405 nm (PL2, dashed curves). The shapes of PL spectra were fitted using Gaussian functions. Resultantly, we obtained the Q, I_{2s} , and D bands analogous to the discussed above ones (the I_{1s} band is almost completely overlapped by the Q band). It can be seen that the magnitude of the Stokes shift between the PLE and PL1 bands equals $\Delta_0 \approx 160 \text{ meV}$, and the origin of its formation differs from that in the case of solution. In the film, strong interaction between QDs leads to delocalization of excitons and their tunneling into large QDs, where they recombine to form the Q band. The reason of exciton localization in such QDs is the substantial mitigation of the quantum-size effect at the tunneling process and the exponential decrease of their wave function amplitude outside the QD.

Again, making use of the particle-in-a-sphericalbox model, we estimated the QD radius that corresponds to the Q band: $R_3 \approx 2.1 \pm 0.1$ nm. The obtained result indicates that, unlike the solutions, the Stokes shift in QD films occurs due to the diffusion of excitons into the QDs with R_3 , where they recombine. Further, a comparison of the positions of the IGS bands and defect states in the film and the solution shows that they do not change their positions, which means that these states do not depend on either the QD size or the excitation energy. However, at resonant excitation with $\lambda_{\rm exc} \approx 405$ nm, cold excitons are created, and, due to fast relaxation and small energy losses, they populate the I_{2s} and D states. Therefore, the integral areas A of these bands at various excitation energies increase significantly. Now, their ratios are $A(I_{2s}, 405 \text{ nm})/A(I_{2s}, 255 \text{ nm}) \approx 7.4 \text{ and}$ $A(D, 405 \text{ nm})/A(D, 255 \text{ nm}) \approx 1.1.$

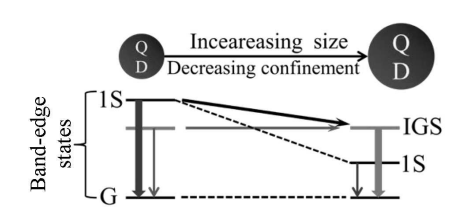
The QD-size independence of IGS states has an important consequence, which is explained in Scheme 2. At certain QD sizes, the quantum 1S and IGS states

of excitons can be in resonance, but at larger QD sizes, the IGS becomes higher by energy. Using the particle-in-a-spherical-box model, we calculated the radii of QDs at which their quantum 1S exciton level is in resonance with the I_{1s} ($R_{1s}\approx 1.9\pm 0.2$ nm) or the I_{2s} ($R_{2s}\approx 2.8\pm 0.2$ nm) level. Whence, two results follow.

- (i) The resonance of states can significantly enhance the process of electronic excitation energy transfer in the film by increasing the density of states participating in this process.
- (ii) For QDs with $R \geq R_{2s}$, the PL will be caused mainly by the emission from IGS states (the thick blue arrow on the right side of Scheme 2), therefore the contribution of quantum states will be insignificant (the thin red arrow).

This may impose a restriction on the range of QD sizes because the quantum-size effect of excitons will cease to be realized at the indicated radii, and the application of such QDs will not make sense.

Now, let us analyze the internal relaxation processes of excitons in the QD film (accompanied by the energy transfer) and isolated QDs, and estimate the QD radius at which the rates of those processes coincide. In Fig. 8 shows the PL spectra of the QD film with R_1 at excitation with various wavelengths (energies). The entire spectra can be conventionally divided into three parts: (I) quantum states, (II) IGS, and (III) surface (defect) states. The figure shows that at the excitation with a high excess energy $(\approx 1450 \text{ meV})$, due to the energy transfer, the PL intensity from quantum states substantially exceeds that from parts II and III of the spectrum. In the QD solution, the situation is opposite, and for a similar excess excitation energy, surface (defect) states become quickly populated; just these states are responsible for the broad shape of the PL band (Fig. 4). The PL intensity from the quantum and surface states of QDs in the film become equal only at $\lambda_{\rm exc} \approx 325$ nm, which corresponds to the resonant excitation of QDs with $R_p \approx 1.4$ nm. In other words, starting from $R \approx R_p$, the rates of the energy transfer among QDs and the internal relaxation of excitons begin to coincide due to a decrease in the initial kinetic energy of excitons. The figure also demonstrates that with the increasing excitation wavelength, only a redistribution of PL intensity between the IGS and surface states takes place, and there is no red shift of the bands of these states. These facts suggest that, unlike



Scheme 2. Independence of the IGS level from the QD size leads to a situation when, at a certain QD radius, it will be in resonance with the 1S level. If the QD radius grows further, the IGS level becomes higher by energy than the 1S level. G is the ground level

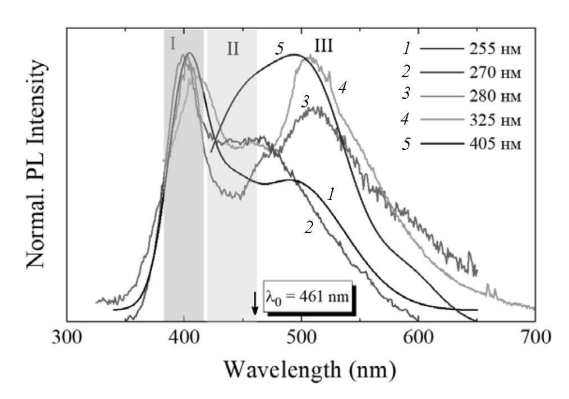


Fig. 8. Normalized PL spectra of the QD film at various excitation wavelengths (indicated in the figure). Sections I, II, and III mark the intervals of quantum (internal) exciton states, IGS states, and surface (defect) states, respectively

the quantum states, the latter have no wide energy distribution (dispersion) and, probably, form single energy levels, whose positions do not depend on the QD size.

The measurements of the time-resolved PL decay profiles at various wavelengths (energies) give an opportunity to understand the dynamic properties of excitons and determine their decay rates in various states. Figure 9 exhibits the PL decay profiles registered at three wavelengths in the case of excitation with a high excess energy (about 1.45 eV) sufficient to create hot excitons, as is shown in the inset. Despite the presence of hot excitons, the excitation energy transfer between the quantum states dominates over the trapping of hot excitons into the IGS and surface states.

For more understanding, the figure shows the registered decay profiles for the state with the excitation energy transfer ($\lambda = 370$ nm) and the radiative states ($\lambda = 403$ and 420 nm). The average (subnanosecond)

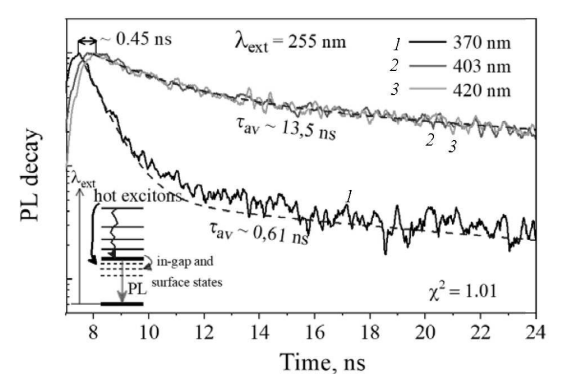


Fig. 9. Profiles of PL decay at wavelengths of 370, 403, and 420 nm under excitation with 255 nm, and average decay times $(\tau_{\rm av})$ obtained by fitting the PL decay profiles with double-exponential functions (the blue dashed curves). The diagram in the inset illustrates the excitation of the system, the formation of hot excitons, and their relaxation path; χ^2 is the fitting quality factor

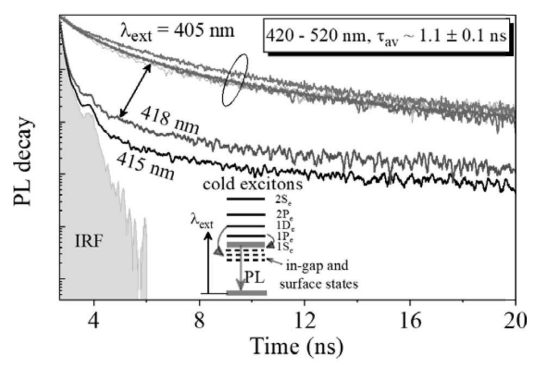


Fig. 10. Profiles of PL decay at wavelengths of 415 and 418 nm, and (for the IGS region and surface states 420÷520 nm) at resonant excitation with 405 nm. $\tau_{\rm av}$ is the average decay time for the latter. The schematic diagram of QD excitation, formation of cold excitons, and their relaxation paths is shown in the inset

decay time obtained for the former state by approximating the decay profile using a double-exponential function (see above) equals $\tau_{\rm av} \approx 0.61$ ns; it is mainly associated with the ultrafast energy transfer among QDs [13, 14].

Figure 9 also shows that the transfer process manifests itself in the decay of PL in small QDs (black curve) and the increase in large ones at $\lambda=403$ (red curve) and 420 nm (green curve). These facts make it possible to determine the rate of excitation energy transfer in QD films, namely, about 2.2 ns⁻¹. The rapid capture of hot excitons into the radiative and surface states makes the corresponding decay profiles

inseparable, and the average decay time increases to $\tau_{\rm av}\approx 13.5~\rm ns.$

The decay dynamics changes drastically under long-wave excitation with $\lambda_{\rm exc} = 405$ nm (3.06 eV), which enters into resonance with the 1S level of the QD and excites cold excitons, as is shown in Fig. 10. Their relaxation into the 1S state of QDs is extremely fast, so the decay times for the interval $\lambda \approx (410$ – 418) nm are beyond the resolution of our instrument (about 200 ps). However, in the interval 418–420 nm, we can observe some kind of "gap" (marked by an arrow): a sharp increase of the average decay time to $\tau_{\rm av} = (1.1 \pm 0.1)$ ns. In the interval 420–520 nm, the profiles strongly overlap, so the average decay time almost does not change. The effective-mass model makes it possible to determine the QD size corresponding to the 1S state of excitons with $\lambda = 420 \text{ nm}$ (2.95 eV); it equals $R_m = (2.5 \pm 0.1) \text{ nm. The most}$ acceptable explanation for this sharp increase of the average decay time (the appearance of a "gap") of the latter is as follows. Starting from this QD radius value, the wave functions of the quantum and IGS states overlap. As a result, the rapid capture of excitons into the IGS states makes the stationary PL dependent exclusively on them, so the decay profiles in the interval $\lambda > 420$ nm strongly overlap, and the value of τ_{av} almost does not change, as is shown in Fig. 10.

As was explained in Scheme 2, this process can have two important consequences:

- 1) in QDs with $R > R_m$, PL is associated with the IGS states rather than the quantum ones;
- 2) the presence of the IGS states restricts the size and number of QDs that can participate in the process of excitation energy transfer.

Unlike the authors of work [12], we believe that excitons localized in the IGS states cannot transfer excitation energy due to their strong localization and the weak overlap of wave functions between neighboring QDs. As a result, QDs with $R_m \approx 2.5$ nm are probably the largest ones where the lowest quantum exciton state determines their PL and excitation energy transfer. However, this conclusion requires further research.

4. Conclusions

By comparing the steady-state and time-resolved PL spectra of colloidal solutions and solid films of ZnSe

QDs, we obtained important results concerning the transformation of quantum, IGS, and surface excitonic states when changing from one system to the other. We showed that in the QD solution and film, such phenomena as the Stokes shift and the rate of internal exciton relaxation are of different origins; in particular, in the film, they depend on the strong interaction between excitons in QDs. The transfer of excitation energy between the QD donors and acceptors was experimentally shown, and the rate of this process in a system with the energy and spatial disorders was determined. Another important result consists in that the IGS states of charge carriers (excitons) do not depend on the QD size and can be in resonance with the quantum QD state at certain QD sizes, in this way enhancing the process of excitonic excitation energy transfer. Thus, the obtained results give an idea of the evolution of excitonic processes when changing from ZnSe-QD solutions to ZnSe-QD solid films, which may bring us closer to the creation of photovoltaic structures and light-harvesting complexes with the parameters of natural photosynthetic mechanisms.

- J. Lihong, S.V. Kershaw, L. Yilin, H. Xiaodan, L. Yingying, A.L. Rogach, G. Mingyuan. Aqueous based semiconductor nanocrystals. *Chem. Rev.* 116, 10623 (2016).
- C.L. Bassani et al. Nanocrystal assemblies: current advances and open problems. ACS Nano 18, 14791 (2024).
- N. Hildebrandt et al. Energy transfer with semiconductor quantum dot bioconjugates: a versatile platform for biosensing, energy harvesting, and other developing applications. Chem. Rev. 117, 536 (2017).
- D. Perera, R. Lorek et al. Photocatalytic activity of core/shell semiconductor nanocrystals featuring spatial separation of charges. J. Phys. Chem. C 116, 22786 (2012).
- T. Mirkovic, E.E. Ostroumov, J.M. Anna, R. van Grondelle, G.D. Scholes. Light absorption and energy transfer in the antenna complexes of photosynthetic organisms. *Chem. Rev.* 117, 249 (2017).
- G. Shi et al. The effect of water on colloidal quantum dot solar cells. Nat. Comm. 12, 4381 (2021).
- L. Yun, K. Donghun, P.M. Owen, D. Zhitomirsky, J.C. Grossman. Origins of the stokes shift in PbS quantum dots: impact of polydispersity, ligands, and defects. ACS Nano 12, 2838 (2018).
- Hua Li et al. Elucidating the mechanisms of the large stokes shift in isolated and coupled PbS quantum dots. J. Phys. Chem. C 128, 8732 (2024).
- 9. M.V. Bondar, M.S. Brodyn, Y.P. Pyryatynskyi, N.A. Matveevska. Stationary spectroscopy and sub-nanosecond res-

- onant energy transfer of exciton excitation of aqueous solutions and films of ZnSe nanocrystals. *Ukr. J. Phys.* **67**, 544 (2022).
- O. Voznyy et al. Origins of Stokes shift in PbS nanocrystals. Nano Lett. 17, 7191 (2017).
- M. C. Brennan, J.E. Herr, T.S. Nguyen-Beck, J. Zinna, S. Draguta, S. Rouvimov, J. Parkhill, M. Kuno. Origin of the size-dependent Stokes shift in CsPbBr₃ perovskite nanocrystals J. Am. Chem. Soc. 139, 12201 (2017).
- Th.A. Klar, Th. Franzl, A.L. Rogach, J. Feldmann. Superefficient exciton funneling in layer-by-layer semiconductor nanocrystal structures. Adv. Mater. 17, 769 (2005).
- N.V. Bondar, M.S. Brodyn, N.A. Matveevskaya, T.G. Beynik. Efficient and sub-nanosecond resonance energy transfer in close-packed films of ZnSe quantum dots by steady-state and time-resolved spectroscopy. Superlatt. Microstruct. 130, 106382 (2020).
- 14. N.V. Bondar, Yu.P. Pyryatynsky. Arrays of size-dispersed ZnSe quantum dots as artificial antennas: role of quasicoherent regime and in-gap states of excitons for enhanced light harvesting and energy transfer. Curr. Appl. Phys. 48, 114 (2023).
- J. Giblin, M. Kuno. Nanostructure absorption: a comparative study of nanowire and colloidal quantum dot absorption cross sections. J. Phys. Chem. Lett. 1, 3340 (2010).
- Qiuyang Li, Kaifeng Wu, Haiming Zhu, Ye Yang, Sheng He, Tianquan Lian. Charge transfer from quantum-confined 0d, 1d, and 2d nanocrystals. *Chem. Rev.* 124, 5695 (2024).
- N.C. Anderson, M.P. Hendricks, J.J. Choi, J.S. Owen. Ligand exchange and the stoichiometry of metal chalcogenide nanocrystals: spectroscopic observation of facile metal-carboxylate displacement and binding. J. Am. Chem. Soc. 135, 18536 (2013).
- S.F. Wuister, C. de Mello Donega, A. Meijerink. Influence of thiol capping on the exciton luminescence and decay kinetics of CdTe and CdSe quantum dots. J. Phys. Chem. B. 108, 17393 (2004).
- J. Eilers, J. van Hest, A. Meijerink, C. de Mello Donega. Unravelling the size and temperature dependence of exciton lifetimes in colloidal ZnSe quantum dots. J. Phys. Chem. C. 118, 23313 (2014).
- D.H. Nguyen, Sung Hun Kim, Joon Sue Lee, Dong Su Lee, Hong Seok Lee. Reaction-dependent optical behavior and theoretical perspectives of colloidal ZnSe quantum Dots. Sci. Rep. 14, 13982 (2024).
- R. Toufanian, Z. Xingjian, J.C. Kays, A.M. Saeboe, A.M. Dennis. Correlating ZnSe quantum dot absorption with particle size and concentration. *Chem. Matt.* 33, 7527 (2021).
- R. Yousefi, H.R. Azimi, M.R. Mahmoudian, W.J. Basirun. The effect of defect emissions on enhancement photocatalytic performance of ZnSe QDs and ZnSe/rGO nanocomposites. Appl. Surf. Sci. 435, 886 (2018).

- 23. Desong Guo et al. Doping of Mn²⁺ into aqueous ZnSe nanocrystals with pure dopant emission through a light-induced electrostatic attraction and diffusion method. J. Phys. Chem. C. 125, 989 (2021).
- C.S. Ponseca, Jr., P. Chabera, J. Uhlig, P. Persson, V. Sundström. Ultrafast electron dynamics in solar energy conversion. *Chem. Rev.* 117, 10940 (2017).
- P.C. Sercel, Al.L. Efros, M. Rosen. Intrinsic gap states in semiconductor nanocrystals. *Phys. Rev. Lett.* 83, 2394 (1999).
- Y. Zhang, D. Zherebetskyy, N.D. Bronstein, S. Barja,
 L. Lichtenstein, A.P. Alivisatos, Lin-Wang Wang, M. Salmeron. Molecular oxygen-induced in-gap states in PbS quantum dots. ACS Nano 9, 10445 (2015).
- Zaiping Zeng et al. Size engineering of trap effects in oxidized and hydroxylated ZnSe quantum dots. Nano Lett. 22, 3604 (2022).
- Zaiping Zeng et al. Bulk-like ZnSe quantum dots enabling efficient ultranarrow blue light-emitting diodes. Nano Lett. 21, 7252 (2021).
- M. Abdellah, K.J. Karki, N. Lenngren et al. Ultra longlived radiative trap states in CdSe quantum dots. J. Phys. Chem. C 118, 21682 (2014).
- T. Hanrath. Colloidal nanocrystal quantum dot assemblies as artificial solids. J. Vac. Sci. Technol. A 30, 030802 (2013).
- R.D. Harris, S.B. Homan et al. Electronic processes within quantum dot-molecule complexes. Chem. Rev. 116, 12865 (2016).
- W. Jaskolski, G.W. Brayany et al. Artificial molecules. Quant. Chem. 90, 1075 (2002).

 N. Kholmicheva, P. Moroz, H. Eckard, G. Jensen, M. Zamkov. Energy transfer in quantum dot solids. ACS Energy Lett. 2, 154 (2017).

Received 07.12.24

М.В. Бондар, Ю.П. Пирятинський, О.В. Твердохлібова ПОРІВНЯЛЬНІ ОПТИЧНІ ТА ЕНЕРГЕТИЧНІ ХАРАКТЕРИСТИКИ ЕКСИТОНІВ У ВОДНИХ РОЗЧИНАХ ТА ТВЕРДИХ ПЛІВКАХ КВАНТОВИХ ТОЧОК

В роботі наведено результати досліджень колоїдних розчинів надмалих квантових точок (KT) ZnSe та їх щільних плівок, які є матеріальною основою оптоелектронних приладів. Порівняння результатів розчинів та плівок дозволяє краще зрозуміти трансформацію їх оптичних характеристик при переході від системи невзаємодіючих частинок у розчині до системи з сильною екситонною взаємодією між КТ. Делокалізація екситонів та гібридизація їх хвильових функцій створюють у плівках новий набір енергетичних станів КТ, які визначають їх оптичні та транспортні характеристики. Ми виявили значний червоний зсув між спектрами поглинання розчину та плівки, природа якого зумовлена сильною взаємодією між КТ. Досліджені динамічні характеристики показали, що час переносу енергії збудження екситонів у плівках KT ZnSe із сильною взаємодією може бути субнаносекундним (~610 пс) і переважати час внутрішньої релаксації екситонів у внутрішньощілинні, поверхневі та дефектні стани носіїв заряду.

Knnuosi c.nosa: Стоксів зсув, квантова точка, енергія збудження, екситон, ZnSe.